A finite element method with overlapping meshes for free-boundary axisymmetric plasma equilibria in realistic geometries

Holger Heumann, Francesca Rapetti

A finite element method with overlapping meshes for free-boundary axisymmetric plasma equilibria in realistic geometries

Holger Heumann, Francesca Rapetti

RESEARCH REPORT
N° 8916
27.5.2016
Project-Teams CASTOR

ISSN 0249-6399 ISRN INRIA/RR--8916--FR+ENG

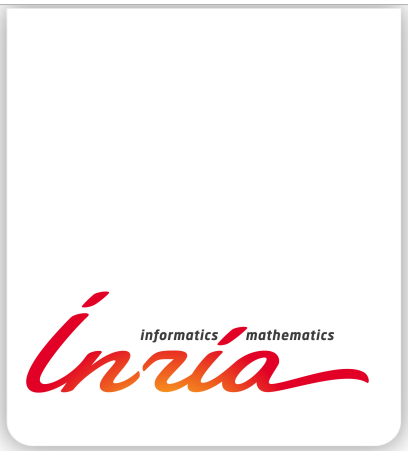

A finite element method with overlapping meshes for free-boundary axisymmetric plasma equilibria in realistic geometries

Holger Heumann, Francesca Rapetti

Project-Teams CASTOR

Research Report n° 8916 — 27.5.2016 — 24 pages

Abstract: Existing finite element implementations for the computation of free-boundary axisymmetric plasma equilibria approximate the unknown poloidal flux function by standard lowest order continuous finite elements with discontinuous gradients. The location of critical points of the poloidal flux, that are of paramount importance in tokamak engineering, is constrained to nodes of the mesh, which leads to undesired jumps in transient problems. Moreover, recent numerical results for the self-consistent coupling of equilibrium with resistive diffusion and transport suggest the necessity of higher regularity when approximating the flux map. In this work we propose a mortar element method that employs two overlapping meshes. One mesh with Cartesian quadrilaterals covers the vacuum domain and one mesh with triangles discretizes the region outside the vacuum domain. The two meshes overlap in a narrow region around the vacuum domain. This approach gives the flexibility to achieve easily and at low cost higher order regularity for the approximation of the flux function in the domain covered by the plasma, while preserving accurate meshing of the geometric details exterior to the vacuum. The continuity of the numerical solution in the region of overlap is weakly enforced by a mortar-like projection.

Key-words: axisymmetric plasma equilibria in tokamaks; domain decomposition mortar method; overlapping meshes; linear and cubic

RESEARCH CENTRE
SOPHIA ANTIPOLIS – MÉDITERRANÉE

2004 route des Lucioles - BP 93
06902 Sophia Antipolis Cedex

Résumé : Pas de résumé

Mots-clés : Pas de motclef

1 Introduction

Computing plasma equilibria is maybe the most fundamental step in modeling for magnetic fusion applications. Main algorithmic approaches to the axisymmetric equilibrium problems were developed long time ago (we can refer to text books like [7] or [32] for details and references).

In general one differentiates between the so-called free-boundary problem and the fixed-boundary problem. The fixed boundary problem is a semi-linear elliptic boundary value problem in the plasma domain with imposed Dirichlet data at the plasma/vaccum interface (which is assumed known, in this case). The most recent achievements [30, 40] for this kind of equilibrium problem propose to use higher order/spectral methods to describe with high accuracy the physical field. Higher order/spectral methods [17, 44, 33] are well-established approaches to approximate the solution of linear and non-linear elliptic boundary valued problems. They require isoparametric mappings to guarantee the accuracy of the approximation as soon as the computational domain contains non-polygonal boundaries, as it occurs with the plasma modeling. The less canonical approach to higher order methods for the fixed boundary equilibrium problem in [41] uses approximations of conformal mappings (see also [20]), nevertheless it does not cover the very important case of plasma boundaries with corners. To tackle the fixed boundary equilibrium with prescribed curved boundary in the frame of high order methods is mainly an issue of proficiency in numerical methods for partial differential equations. It is indeed important to stress that the boundary of the plasma is not known a priori. Assuming an arbitrarily detailed knowledge of the plasma boundary is not realistic for the actual physical application. The boundary is either deduced from measurements through experiments combined with reconstruction procedures or it is the output of the free-boundary equilibrium problem. In the latter case, which is the focus of this article, we have to solve a semi-linear elliptic problem in an unbounded domain where the region covered by the plasma is not known. Hence, it is of practical relevance to have numerical methods being to a very high degree independent of the actual plasma boundary.

In this work we will focus on the free-boundary problem and propose an extension of the finite element method introduced in [10] (see also [28]). A very important application for the free-boundary problem is the so-called self-consistent coupling of equilibrium with resistive diffusion and transport [23] that allows to simulate the evolution of the plasma equilibrium over very long time scales. The ability to model in a numerically cheap and practical way the movement of the plasma/vacuum interface during the evolution of the plasma equilibrium is an issue of physical interest. Such simulations are essential for in silico studies of experiments in tokamaks but it turns out that the standard finite element approach with piecewise polynomial, globally continuous approximations has two main drawbacks: 1.) The definition of the plasma boundary hinges on the critical points of the unknown and as the derivatives are not continuous, these points will not move in a continuous way during the evolution. 2.) The resistive diffusion and transport are described by one-dimensional equations containing metric coefficients that depend on the gradient of the solution of the equilibrium problem. These coefficients are not well-defined if the gradients are not continuous.

Hence, in this work we propose a very practical approach that allows to achieve easily continuous differentiability where it is beneficial but stays with the standard methods in the rest of the domain.

In general it is very cumbersome to define finite element spaces that allow for globally continuous differentiability. If one keeps along with triangular meshes, the reduced quintic element [2] is the lowest order element with this property. Reduced quintic elements were introduced for fusion applications firstly in [31]. In the case of Cartesian meshes however, continuous differentiability can be easily achieved with lower order polynomials. By taking tensor products of one dimensional spline basis functions of polynomial order three we end up with a finite element

space of piecewise bicubic polynomials with continuous derivatives, also known as the Bogner-Fox-Schmit element [11, 14]. Inspired by [13] we present a finite element method that employs two meshes, one of rectangles in the vacuum domain, the domain that is accessible by the plasma, and one of triangles outside. This approach gives the flexibility to achieve easily and at low cost higher order regularity for the approximation of the flux function in the domain covered by the plasma, while preserving accurate meshing of the geometric details exterior to the vacuum. As it is impossible to align the boundary of the mesh of rectangles with the interface between vacuum and exterior domain, we will allow for an *overlap* in a narrow region around the interface. The continuity of the numerical solution in the region of overlap is weakly enforced by relying on a mortar-like projection.

The outline for the rest of the article is the following: The next two sections introduce the axisymmetric plasma equilibrium problem and present a weak formulation in a domain decomposition spirit with two distinct domains, the vacuum region and the exterior region. Section 4 is devoted to the presentation of the numerical method combing linear finite elements for the exterior domain and the Bogner-Fox-Schmit element for the vacuum region. Continuity is weakly enforced via a mortar-like method. Section 5 presents a few applications from nuclear fusion science. We end with a short summary and outlook on perspectives.

2 Free-Boundary Equilibrium of Toroidal Plasma

The essential equations for describing plasma equilibrium in a tokamak are force balance, the solenoidal condition and Ampère's law that read respectively

$$\operatorname{grad} p = \mathbf{J} \times \mathbf{B}, \qquad \operatorname{div} \mathbf{B} = 0, \qquad \operatorname{curl} \frac{1}{\mu}\mathbf{B} = \mathbf{J}, \tag{1}$$

where p is the plasma kinetic pressure, $\mathbf{B}$ is the magnetic induction, $\mathbf{J}$ is the current density and μ the magnetic permeability. In the quasi-static approximation these equations are augmented by Faraday's law in all other conducting structures, and by Ohm's laws in plasma, coils and passive structures.

For the considered setting, axial symmetry is a perfectly valid approximation and it is convenient to formulate (1) in a cylindrical coordinate system (r, φ, z) in order to consider only a section at $\varphi =$ constant of the tokamak, generally referred to as poloidal section, to distinguish it from the toroidal section at $r = constant$. We recall that $(x, y, z) \to (r, \varphi, z)$ by the transformation[1] $x = r\cos\varphi$ and $y = r\sin\varphi$. Working in a poloidal section, the scalar field p does not depend on the angle φ, thus ∇p belongs to the poloidal (r, z)-plane. We introduce $\Omega_\infty = [0, \infty] \times [-\infty, \infty]$, the positive half plane, to denote the meridian plane that contains the tokamak centered at the origin. The geometry of the tokamak determines the various subdomains (see Fig. **??**):

- the domain $\Omega_{\mathrm{Fe}} \subset \Omega_\infty$ corresponds to those parts that are made of iron; for an air-transformer tokamak $\Omega_{\mathrm{Fe}} = \emptyset$;

[1] We thus have a transformation in reference system, from $(\mathbf{e}_x, \mathbf{e}_y, \mathbf{e}_z)$ to $(\mathbf{e}_r, \mathbf{e}_\varphi, \mathbf{e}_z)$

$$\mathbf{e}_x = \mathbf{e}_r\cos\varphi - \mathbf{e}_\varphi\sin\varphi, \qquad \mathbf{e}_y = \mathbf{e}_r\sin\varphi + \mathbf{e}_\varphi\cos\varphi,$$

and in the partial derivatives for any scalar field p, from $(\partial_x p, \partial_y p)$ to $(\partial_r p, \partial_\varphi p)$, as follows

$$\partial_x p = \partial_r p\ \cos\varphi - \partial_\varphi p\ \tfrac{\sin\varphi}{r}, \qquad \partial_y p = \partial_r p\ \sin\varphi + \tfrac{1}{r}\partial_\varphi p\ \sin\varphi$$

so that $\nabla p = \mathbf{e}_r\partial_r p + \mathbf{e}_\varphi \frac{1}{r}\partial_\varphi p + \mathbf{e}_z\partial_z p$.

- the domains $\Omega_{c_i} \subset \Omega_\infty$, $1 \le i \le N$, correspond to the N poloidal field coils. The intersection of the ith coil with the poloidal plane is Ω_{c_i}, and it has n_i wire turns, total resistance R_i and cross section area $|\Omega_{c_i}|$;

- the domain $\Omega_L \subset \Omega_\infty$, bounded by the limiter, corresponding to the domain which is accessible by the plasma;

- the domain $\Omega_p \subset \Omega_L$, corresponding to the domain covered by the plasma.

The classical primal unknowns for toroidal plasma equilibria described by (1) are the *poloidal magnetic flux* $\psi = \psi(r,z)$, the pressure p and the *diamagnetic function* f. The poloidal magnetic flux $\psi := r\mathbf{A}\cdot\mathbf{e}_\varphi$ is the scaled toroidal component of the vector potential $\mathbf{A}$, i.e. $\mathbf{B} = \operatorname{curl}\mathbf{A}$ and $\mathbf{e}_\varphi$ the unit vector for φ. The diamagnetic function $f = r\mathbf{B}\cdot\mathbf{e}_\varphi$ is the scaled toroidal component of the magnetic field. It can be shown that both the pressure p and the diamagnetic function f are constant on ψ-isolines, i.e. $p = p(\psi)$ and $f = f(\psi)$. We refer to standard text books, e.g. [18], [7], [47], [22], [21] and [32] for the details and state in the following paragraphs only the final equations.

Force balance, solenoidal condition and Ampère's law in (1) yield, in axisymmetric configuration, the following set of equations for the flux $\psi(r,z)$:

$$\begin{aligned} -\nabla\cdot\left(\tfrac{1}{\mu r}\nabla\psi\right) &= \begin{cases} rp'(\psi) + \frac{1}{\mu_0 r} f f'(\psi) & \text{in } \Omega_p(\psi)\,; \\ I_i/|\Omega_{c_i}| & \text{in } \Omega_{c_i}\,; \\ 0 & \text{elsewhere in } \Omega_\infty\,, \end{cases} \\ \psi(0,z) = 0\,; \qquad & \lim_{\|(r,z)\|\to+\infty} \psi(r,z) = 0\,; \end{aligned} \tag{2}$$

where ∇ is the gradient in the half plane Ω_∞, I_i is the total current (in At, Ampère turns) in the ith coil and μ is a functional of ψ

$$\mu = \begin{cases} \mu_{\mathrm{Fe}}(\frac{|\nabla\psi|^2}{r^2}) & \text{in } \Omega_{\mathrm{Fe}} \\ \mu_0 & \text{elsewhere}\,, \end{cases} \tag{3}$$

with μ_0 the constant magnetic permeability of vacuum and μ_{Fe} the non-linear magnetic permeability of iron. Here again, we would like to stress that the plasma domain $\Omega_p(\psi)$ is an unknown, which depends non-linearly on the magnetic flux ψ: the plasma domain $\Omega_p(\psi)$ is a functional of the poloidal flux ψ. The different characteristic shapes of $\Omega_p(\psi)$ are illustrated in Figure **??**: the boundary of $\Omega_p(\psi)$ either touches the boundary of Ω_L (limiter case) or the boundary contains one or more saddle points of ψ (divertor configuration). The saddle points of ψ, denoted by (r_X, z_X)=$(r_X(\psi), z_X(\psi))$, are called X-points of ψ. The plasma domain $\Omega_p(\psi)$ is the largest subdomain of Ω_L bounded by a closed ψ-isoline in Ω_L and containing the magnetic axis (r_{ax}, z_{ax}). The magnetic axis is the point $(r_{ax}, z_{ax}) = (r_{ax}(\psi), z_{ax}(\psi))$, where ψ has its global maximum in Ω_L. For convenience, we introduce also the coordinates $(r_{bd}, z_{bd}) = (r_{bd}(\psi), z_{bd}(\psi))$ of the point that determines the plasma boundary. Note that (r_{bd}, z_{bd}) is either an X-point of ψ or the contact point with the limiter $\partial\Omega_L$.

The equation (2) in the plasma domain, i.e.

$$-\partial_r\left(\frac{1}{\mu_0 r}\partial_r\psi\right) - \partial_z\left(\frac{1}{\mu_0 r}\partial_z\psi\right) = rp'(\psi) + \frac{1}{\mu_0 r} f f'(\psi), \tag{4}$$

is the celebrated *Grad-Shafranov-Schlüter* equation [24, 45, 36]. The domain of p' and $f\,f'$ is the interval $[\psi_{bd}, \psi_{ax}]$ with the scalar values ψ_{ax} and ψ_{bd} being the flux values at the *magnetic axis*

and at the boundary of the plasma:

$$\begin{aligned}\psi_{\rm ax}(\psi) &:= \psi(r_{\rm ax}(\psi), z_{\rm ax}(\psi))\,,\\ \psi_{\rm bd}(\psi) &:= \psi(r_{\rm bd}(\psi), z_{\rm bd}(\psi))\,.\end{aligned} \tag{5}$$

The two functions p' and $f\,f'$ and the currents I_i in the coils are not determined by the model (2) and have to be supplied as data. Since the domain of p' and $f\,f'$ depends on the poloidal flux itself, it is more practical to supply those profiles as functions of the normalized poloidal flux $\psi_{\rm N}(r,z)$:

$$\psi_{\rm N}(r,z) = \frac{\psi(r,z)-\psi_{\rm ax}(\psi)}{\psi_{\rm bd}(\psi)-\psi_{\rm ax}(\psi)}\,. \tag{6}$$

These two functions, subsequently termed $S_{p'}$ and $S_{ff'}$, have, independently of ψ, a fixed domain $[0,1]$. They are usually given as piecewise polynomial functions. Another frequent a priori model is

$$S_{p'}(\psi_{\rm N}) = \lambda\frac{\beta}{r_0}(1-\psi_{\rm N}^{\alpha})^{\gamma}\,,\quad S_{ff'}(\psi_{\rm N}) = \lambda(1-\beta)\mu_0 r_0(1-\psi_{\rm N}^{\alpha})^{\gamma}\,, \tag{7}$$

with r_0 the major radius (in meters) of the vacuum chamber and $\alpha,\beta,\gamma\in\mathbb{R}$ given parameters. We refer to [37] for a physical interpretation of these parameters. The parameter β is related to the poloidal beta [7, p. 15], whereas α and γ describe the peakage of the current profile, λ is a scaling parameter related to the total plasma current.

As we are going to present later a discretization scheme for the problem (2) that employs different approximation spaces on $\Omega_{\rm L}$ and its complement $\Omega^{\rm ex}=\Omega\setminus\Omega_{\rm L}$ we formulate the variational problem directly in a domain decomposition framework.

3 Weak Formulation

We chose a semi-circle Γ of radius ρ_Γ surrounding the iron domain $\Omega_{\rm Fe}$ and the coil domains Ω_{c_i}. The truncated domain, we use for the computations, is the domain $\Omega\subset\Omega_\infty$ having the boundary $\partial\Omega=\Gamma\cup\Gamma_0$, where $\Gamma_0:=\{(0,z),\,-\rho_\Gamma\le z\le\rho_\Gamma\}$. Let $L^2_*(\Omega)$, be the functional space[2]

$$L^2_*(\Omega) = \{g:\Omega\to\mathbb{R},\quad \|g\|^2_{*,\Omega} := \int_\Omega g^2 r^{-1}drdz<\infty\}$$

and $\mathcal{H}^1(\Omega)=\{u\in L^2_*(\Omega),\ \nabla u\in L^2_*(\Omega)^2\}$ the Hilbert space endowed with the norm $\|u\|^2_{\mathcal{H}^1(\Omega)} = \|u\|^2_{*,\Omega}+|u|^2_{\mathcal{H}^1(\Omega)}$ where $|u|^2_{\mathcal{H}^1(\Omega)} = \|\partial_r u\|^2_{*,\Omega}+\|\partial_z u\|^2_{*,\Omega}$. For $\psi\in\mathcal{H}^1(\Omega)$ the trace on Γ_0 vanishes in the following sense [27]

$$\lim_{r\to 0^+}\int_{[-\rho_\Gamma,\rho_\Gamma]\cap\Omega} r^{-2}\psi(r,z)^2dz = 0\,.$$

To formulate for (2) a variational problem in a domain decomposition framework, let us introduce the functional space

$$\mathcal{V} = \{(v,w)\in\mathcal{H}^1(\Omega^{\rm ex})\times(\mathcal{H}^1(\Omega_{\rm L})\cap C^0(\Omega_{\rm L})),\ v_{|\Gamma_0}=0,\ v_{|\gamma}=w_{|\gamma}\}.$$

We require continuity in $\Omega_{\rm L}$ to have meaningful $\psi_{\rm ax}$ and $\psi_{\rm bd}$ that appear in the definition of $\Omega_{\rm p}$ and $\psi_{\rm N}$. Then, the weak formulation of (2) is: Find $(\psi_{\rm ex},\psi_L)\in\mathcal{V}$ s.t.

$$\mathsf{a}((\psi_{\rm ex},\psi_L),(v,w)) = \ell(\vec{I},v)\quad\forall(v,w)\in\mathcal{V}. \tag{8}$$

[2]Let $H(\mathrm{curl},\Omega\times[0,2\pi])$ be the space of vector fields in $L^2(\Omega\times[0,2\pi])^3$ with curl in $L^2(\Omega\times[0,2\pi])^3$. We remark that: $r^{-1}\psi\mathbf{e}_\phi\in H(\mathrm{curl},\Omega\times[0,2\pi])$ if and only if $\psi\in\mathcal{H}^1(\Omega)$.

In (8), we have set

$$\begin{aligned}
\mathsf{a}((\psi_{\rm ex},\psi_L),(v,w)) &:= \mathsf{a}^{\rm ex}(\psi_{\rm ex},v)+\mathsf{a}^{\rm L}(\psi_L,w),\\
\mathsf{a}^{\rm ex}(\psi,v) &:= \int_{\Omega^{\rm ex}} \frac{1}{\mu(\psi)r}\nabla\psi\cdot\nabla v\,drdz+\mathsf{c}(\psi,v),\\
\mathsf{a}^{\rm L}(\psi,w) &:= \int_{\Omega_{\rm L}} \frac{1}{\mu_0 r}\nabla\psi\cdot\nabla w\,drdz-\ \mathsf{J}_{\rm p}(\psi,w),
\end{aligned}$$

where

$$\begin{aligned}
\mathsf{J}_{\rm p}(\psi,\xi) &:= \int_{\Omega_{\rm p}(\psi)}\left(rS_{p'}(\psi_{\rm N})+\frac{1}{\mu_0 r}S_{ff'}(\psi_{\rm N})\right)\xi\,drdz\\
\ell(\vec{I},\xi) &:= \sum_{i=1}^{N}\frac{\vec{I}_i}{|\Omega_{{\rm c}_i}|}\int_{\Omega_{{\rm c}_i}}\xi\,drdz
\end{aligned}\tag{9}$$

and

$$\begin{aligned}
\mathsf{c}(\psi,\xi) := \frac{1}{\mu_0}\int_\Gamma \psi(\mathbf{P}_1)N(\mathbf{P}_1)\xi(\mathbf{P}_1)dS_1\\
+\frac{1}{2\mu_0}\int_\Gamma\int_\Gamma(\psi(\mathbf{P}_1)-\psi(\mathbf{P}_2))M(\mathbf{P}_1,\mathbf{P}_2)(\xi(\mathbf{P}_1)-\xi(\mathbf{P}_2))dS_1dS_2\,,
\end{aligned}\tag{10}$$

with

$$\begin{aligned}
M(\mathbf{P}_1,\mathbf{P}_2) &= \frac{k_{\mathbf{P}_1,\mathbf{P}_2}}{2\pi(r_1r_2)^{\frac{3}{2}}}\left(\frac{2-k^2_{\mathbf{P}_1,\mathbf{P}_2}}{2-2k^2_{\mathbf{P}_1,\mathbf{P}_2}}E(k_{\mathbf{P}_1,\mathbf{P}_2})-K(k_{\mathbf{P}_1,\mathbf{P}_2})\right)\\
N(\mathbf{P}_1) &= \frac{1}{r_1}\left(\frac{1}{\delta_+}+\frac{1}{\delta_-}-\frac{1}{\rho_\Gamma}\right)\ \text{and}\ \delta_\pm=\sqrt{r_1^2+(\rho_\Gamma\pm z_1)^2}\,,
\end{aligned}$$

where $\mathbf{P}_i=(r_i,z_i)$ and K and E the complete elliptic integrals of first and second kind, respectively and

$$k_{\mathbf{P}_j,\mathbf{P}_k}=\sqrt{\frac{4r_jr_k}{(r_j+r_k)^2+(z_j-z_k)^2}}\,.$$

The bilinear form $\mathsf{c}(\cdot,\cdot)$ is accounting for the boundary conditions at infinity [1]. We refer to [25, Chapter 2.4] for the details of the derivation. The bilinear form $\mathsf{c}(\cdot,\cdot)$ follows basically from the so called *uncoupling procedure* in [19] for the usual coupling of boundary integral and finite element methods.

In the case of vanishing plasma, $S_{p'}=S_{ff'}=0$, the weak formulation (8) is the classical problem of non-linear magneto-statics; existence and uniqueness can be established under a monontonicity assumption for μ in iron. The result follows directly from combining those for non-linear magneto-statics in [42] with the results for non-linear problems in unbounded domains [19]. If in addition we had $\Omega_{\rm Fe}=\emptyset$ we would end up with an even simpler linear elliptic problem, for which existence and uniqueness are immediately available [27, 26]. Rigorous existence and uniqueness assertion for the general case are still an open problem. See [46, 3, 8, 39] for some theoretical work related to such results.

4 Finite Element Method with Overlapping Meshes

We wish to use in the domain $\Omega_{\rm L}$ finite element approximations ψ_h for the poloidal flux ψ that are not only continuous but have also continuous gradients $\nabla\psi_h$. This is particularly simple if we

adopt a Cartesian mesh of rectangles in Ω_{L} and use the bicubic Bogner-Fox-Schmit finite element space [11, 14]. The Bogner-Fox-Schmit rectangular element is one of the simplest elements that provide continuous differentiability of the approximate solution. However, it can be applied only on a mesh of rectangles or paralellogramms, hence only to domains with boundaries that are parallel to two different straight directions. As meshes with only rectangular elements are not very suitable for realistic geometry description of the tokamak, we prefer to keep a mesh of triangles and linear Lagrangian finite elements for the exterior domain Ω^{ex}. It is clearly not possible to cover Ω_{L} perfectly with a mesh of rectangular elements, so we accept a certain overlap of the two meshes and use a mortar-like element method (MEM) to enforce weakly continuity of Dirichlet and Neumann traces over the interface. This modified version of MEM has been introduced in [13] for non-distructive testing. A related MEM was introduced earlier in [35] and a convergence analysis of the method for a model problem can be found in [12].

4.1 Preliminary Notation

We assume that the interface $\gamma := \partial\Omega_{\mathrm{L}}$, between the vacuum domain Ω_{L} and the exterior domain Ω^{ex}, is polygonal and introduce a standard mesh τ^{ex} of triangular elements that covers the domain Ω^{ex} exterior to the vacuum domain Ω_{L}. The boundary of Ω^{ex} is $\partial\Omega^{\mathrm{ex}} = \Gamma \cup \Gamma_0 \cup \gamma$. We assume that triangles T_i of τ^{ex} are shape regular and quasi-uniform. Next we introduce a (second, independent) mesh τ^{in} of rectangular elements K_j that covers a domain Ω^{in} such that $\Omega_{\mathrm{L}} \subset \Omega^{\mathrm{in}}$. We assume that Ω^{in} has a non-vanishing overlap with the domain Ω^{ex}, that is, $\Omega^{\mathrm{ov}} := \Omega^{\mathrm{in}} \cap \Omega^{\mathrm{ex}} \neq \emptyset$. Note that $\partial\Omega^{\mathrm{ov}} = \gamma \cup \tilde{\gamma}$ with $\tilde{\gamma} = \partial\Omega^{\mathrm{in}}$. Both γ and $\tilde{\gamma}$ are polygonal lines with nodes and edges from the meshes τ^{ex} and τ^{in}. We use $\mathcal{N}_\gamma$ (resp. $\mathcal{N}_{\tilde{\gamma}}$) to denote the set of all nodes of γ (resp. $\tilde{\gamma}$). Additionally we denote by $\mathcal{N}_{\tilde{\gamma}}^r$ (resp. $\mathcal{N}_{\tilde{\gamma}}^z$) all the nodes of $\tilde{\gamma}$ that belong to an edge of $\tilde{\gamma}$ that is parallel to the r-axis (resp. the z-axis). Moreover, we suppose that $\Omega_{c_i} \cap \Omega^{\mathrm{in}} = \emptyset$, $1 \leq i \leq N$ (together with $\Omega_{\mathrm{Fe}} \cap \Omega^{\mathrm{in}} = \emptyset$ when $\Omega_{\mathrm{Fe}} \neq \emptyset$).

We introduce two finite element spaces over τ^{ex} and τ^{in}

$$V^{\mathrm{ex}} = \{\phi \in C^0(\Omega^{\mathrm{ex}}) : \phi_{|\Gamma_0} = 0, \phi_{|T} \text{ is a polynomial of degree } 1 \; \forall\, T \in \tau^{\mathrm{ex}}\}$$
$$V^{\mathrm{in}} = \{\varphi \in C^1(\Omega^{\mathrm{in}}), \partial^2_{rz}\varphi \in C^0(\Omega^{\mathrm{in}}) : \varphi_{|K} \text{ is a bicubic polynomial } \forall\, K \in \tau^{\mathrm{in}}\}$$

and denote by V_∂^{ex} (resp. V_∂^{in}) the trace space of V^{ex} (resp. V^{in}) on the closed polygonal line γ (resp. $\tilde{\gamma}$), namely, $V_\partial^{\mathrm{ex}} = \{\phi_{|\gamma}, \phi \in V^{\mathrm{ex}}\}$ (resp. $V_\partial^{\mathrm{in}} = \{\varphi_{|\tilde{\gamma}}, \varphi \in V^{\mathrm{in}}\}$). The space V^{ex} is the standard linear Lagrangian finite element space and V^{in} is known as the Bogner-Fox-Schmit finite element space. Then the trace space $V_\partial^{\mathrm{ex}} \subset C^0(\gamma)$ is the span of affine linear functions defined on the mesh over γ that is induced by τ^{ex}. The degrees of freedom of V^{ex} can be chosen to be the nodal values at the nodes of τ^{ex} that are not in Γ_0, and the degrees of freedom of the trace space V_∂^{ex} can be chosen to be the nodal values on nodes in $\mathcal{N}_\gamma$, i.e. the nodes of τ^{ex} that are on γ (see Figure 1, right). For V^{in} the standard choice of global degrees of freedom are the nodal values of the function, its first order partial derivatives and its second order mixed derivatives at the nodes. Then for the degrees of freedom of the Dirichlet trace space $V_\partial^{\mathrm{in}} \subset C^0(\tilde{\gamma})$ one can simply choose the nodal values at nodes of $\tilde{\gamma}$ plus the nodal values of the partial derivative in direction r (or z) if the nodes belongs to a r-axis parallel edge (or z-axis parallel edge) of $\tilde{\gamma}$.

4.2 The two mortar-like projections

Since $v^{\mathrm{ex}}_{|\tilde{\gamma}} \notin V_\partial^{\mathrm{in}}$ (resp. $v^{\mathrm{in}}_{|\gamma} \notin V_\partial^{\mathrm{ex}}$) for $v^{\mathrm{ex}} \in V^{\mathrm{ex}}$ (resp. $v^{\mathrm{in}} \in V^{\mathrm{in}}$) to impose the transmission condition at γ and $\tilde{\gamma}$ at the discrete level we rely on two mortar-like projections. More precisely, it is possible to define two operators $\pi^{\mathrm{in}} : V^{\mathrm{ex}} \to V_\partial^{\mathrm{in}}$ and $\pi^{\mathrm{ex}} : V^{\mathrm{in}} \to V_\partial^{\mathrm{ex}}$ based on the particular choice of degrees of freedom of V_∂^{ex} and V_∂^{in}:

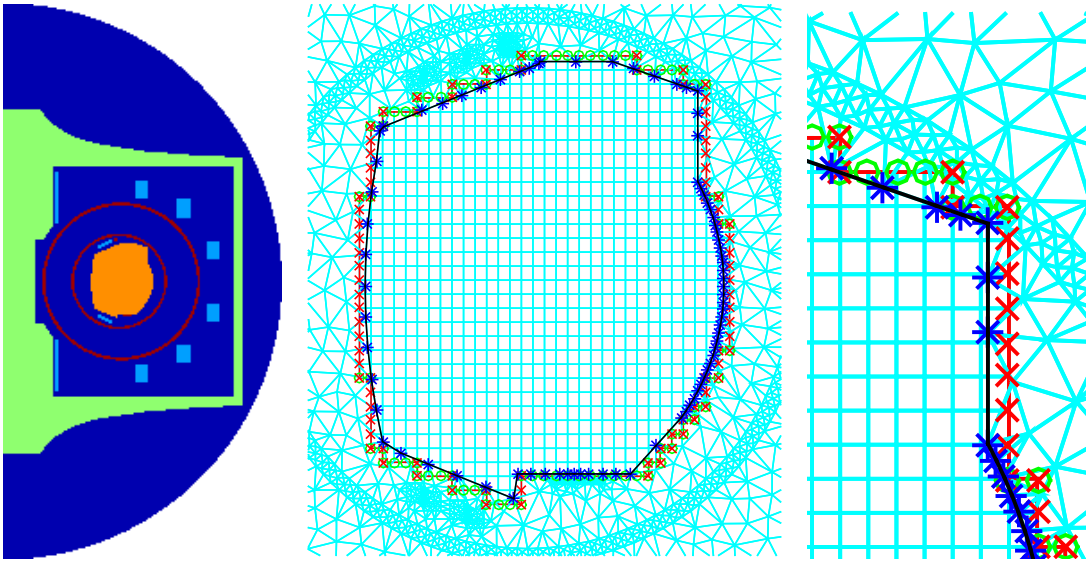

Figure 1: Left: A sketch of the computational domain Ω ($\rho_\Gamma = 5.8m$) and of the different domains for the tokamak WEST. Orange, light blue and Green domains are the vacuum chamber Ω_{L}, the coils Ω_{c_i} and the iron domain Ω_{Fe}. The red domains, the passive structures will be important for transient simulations. Middle and Right: Two close-ups to the vacuum domain Ω_{L} and the two meshes τ^{ex} and τ^{in}. The black and the red lines are γ and $\tilde{\gamma}$. The blue stars correspond to the degrees of freedom of V_∂^{ex}. The red crosses and green circles signify the degrees of freedom of V_∂^{in}. The green circles are the nodes in $\mathcal{N}_{\tilde{\gamma}}^z$, the nodes of $\tilde{\gamma}$ that belong to an edge of $\tilde{\gamma}$ that is parallel to the r-axis, and the red crosses are the nodes in $\mathcal{N}_{\tilde{\gamma}}^r$, the nodes of $\tilde{\gamma}$ that belong to an edge of $\tilde{\gamma}$ that is parallel to the z-axis. Both red crosses and green circles belong to $\mathcal{N}_{\tilde{\gamma}}$

a) For $\psi_{\text{in}} \in V^{\text{in}}$ we define $\pi^{\text{ex}}\psi_{\text{in}} \in V_\partial^{\text{ex}}$ such that

$$(\pi^{\text{ex}}\psi_{\text{in}})(r_i, z_i) := \psi_{\text{in}}(r_i, z_i) \quad \forall \text{ nodes } (r_i, z_i) \in \mathcal{N}_\gamma \,. \tag{11}$$

b) For $\psi_{\text{ex}} \in V^{\text{ex}}$ we define $\pi^{\text{ex}}\psi_{\text{in}} \in V_\partial^{\text{in}}$ such that

$$\begin{aligned} (\pi^{\text{in}}\psi_{\text{ex}})(r_i, z_i) &:= \psi_{\text{ex}}(r_i, z_i) && \forall \text{ nodes } (r_i, z_i) \in \mathcal{N}_{\tilde\gamma} \,, \\ \partial_r(\pi^{\text{in}}\psi_{\text{ex}})(r_i, z_i) &:= \partial_r\psi_{\text{ex}}(r_i, z_i) && \forall \text{ nodes } (r_i, z_i) \in \mathcal{N}_{\tilde\gamma}^r \,, \\ \partial_z(\pi^{\text{in}}\psi_{\text{ex}})(r_i, z_i) &:= \partial_z\psi_{\text{ex}}(r_i, z_i) && \forall \text{ nodes } (r_i, z_i) \in \mathcal{N}_{\tilde\gamma}^z \,. \end{aligned} \tag{12}$$

We remark that π^{in} is not well defined when the nodes $(r_i, z_i) \in N_{\tilde\gamma}^r$ or $(r_i, z_i) \in N_{\tilde\gamma}^z$ happen to lie on an edge of τ^{ex}, since the gradients of functions in V^{ex} are not single valued on edges of τ^{ex}. In the rare cases where we need to manage this multivalued situation, we simply choose one of the possible values.

To enforce the continuity across γ and $\tilde\gamma$ we will make use of two inner products on V_∂^{ex} and V_∂^{in}:

$$\langle \psi, \xi \rangle_\gamma := \sum_{(r_i,z_i)\in\mathcal{N}_\gamma} \psi(r_i, z_i)\xi(r_i, z_i) \quad \psi, \xi \in V_\partial^{\text{ex}}$$

and

$$\begin{aligned} \langle \psi, \xi \rangle_{\tilde\gamma} := &\sum_{(r_i,z_i)\in\mathcal{N}_{\tilde\gamma}} \psi(r_i, z_i)\xi(r_i, z_i) \\ &+ \sum_{(r_i,z_i)\in\mathcal{N}_{\tilde\gamma}^r} \partial_r\psi(r_i, z_i)\partial_z\xi(r_i, z_i) \\ &+ \sum_{(r_i,z_i)\in\mathcal{N}_{\tilde\gamma}^z} \partial_z\psi(r_i, z_i)\partial_z\xi(r_i, z_i) \quad \psi, \xi \in V_\partial^{\text{in}} \end{aligned} \,.$$

4.3 The mortar-like formulation

We are now able to formulate the discrete variational problem, where we enforce continuity via Lagrangian multipliers λ_{ex}, λ_{in}: Find $(\psi_{\text{ex}}, \psi_{\text{in}}) \in V^{\text{ex}} \times V^{\text{in}}$ and $(\lambda^{\text{ex}}, \lambda^{\text{in}}) \in V_\partial^{\text{ex}} \times V_\partial^{\text{in}}$ such that

$$\begin{aligned} \mathsf{a}^{\text{m}}((\psi_{\text{ex}}, \psi_{\text{in}}), (v, w)) + \mathsf{b}((v, w), (\lambda_{\text{ex}}, \lambda_{\text{in}})) &= \ell(\vec{I}, v) && \forall (v, w) \in V^{\text{ex}} \times V^{\text{in}}, \\ \mathsf{b}((\psi_{\text{ex}}, \psi_{\text{in}}), (\nu, \omega)) &= 0, && \forall (\nu, \omega) \in V_\partial^{\text{ex}} \times V_\partial^{\text{in}} \,, \end{aligned} \tag{13}$$

where

$$\begin{aligned} \mathsf{a}^{\text{m}}((\psi_{\text{ex}}, \psi_L), (v, w)) &:= \mathsf{a}^{\text{ex}}(\psi_{\text{ex}}, v) + \mathsf{a}^{\text{in}}(\psi_{\text{L}}, w) \,, \\ \mathsf{a}^{\text{ex}}(\psi, v) &:= \int_{\Omega^{\text{ex}}} \frac{1}{\mu(\psi) r} \nabla\psi \cdot \nabla v \, dr dz + \mathsf{c}(\psi, v) \,, \\ \mathsf{a}^{\text{in}}(\psi, w) &:= \int_{\Omega^{\text{in}}} \frac{1}{\mu_0 r} \nabla\psi \cdot \nabla w \, dr dz - \mathsf{J}_{\text{p}}(\psi, w) \end{aligned} \tag{14}$$

and

$$\mathsf{b}((\psi_{\text{ex}}, \psi_{\text{in}}), (\nu, \omega)) = \langle \psi_{\text{ex}} - \pi^{\text{ex}}\psi_{\text{in}}, \nu \rangle_\gamma + \langle \psi_{\text{in}} - \pi^{\text{in}}\psi_{\text{ex}}, \omega \rangle_{\tilde\gamma} \,.$$

The mappings $\ell(\vec{I}, v)$, $\mathsf{J}_{\text{p}}(\psi, w)$ and $\mathsf{c}(\psi, v)$ are the same as in (9) and (10). The main difference to the method presented in [35] is that we do not introduce weighting coefficients to compensate for the twofold integration over the overlapping domain and hence the consistency error can not be estimated as easily as in [12, Section 4.2]. On the other hand it is this feature that avoids the need to compute the polygonal intersections of triangles and rectangles for the assembling

of $\mathsf{a}^{\rm in}(\psi,w)$ and $\mathsf{a}^{\rm ex}(\psi,v)$. In keeping a non-zero overlap, we expect that the consistency error can be nevertheless controlled. At least the numerical experiments in [13, Section 5.] show convergence of optimal order for a eddy current problem in non-destructive testing using this kind of mortar approach.

Remark 1 *Most of the theoretical work on mortar methods [48, 4] assumes the operators $\pi^{\rm ex}$ and $\pi^{\rm in}$ to be L^2-projections and L^2-inner products are used instead of $\langle\cdot,\cdot\rangle_\gamma$ and $\langle\cdot,\cdot\rangle_{\tilde\gamma}$. It is standard to chose the operator $\pi^{\rm ex}:\mathcal{H}^1(\Omega^{\rm in})\to V_\partial^{\rm ex}$ and $\pi^{\rm in}:\mathcal{H}^1(\Omega^{\rm ex})\to V_\partial^{\rm in}$ as a L^2-orthogonal projections:*

$$\int_\gamma \pi^{\rm ex}\psi\,\xi\,dS=\int_\gamma \psi\,\xi\,dS\quad\forall\xi\in V_\partial^{\rm ex}\,,$$

and

$$\int_{\tilde\gamma} \pi^{\rm in}\psi\,\xi\,dS=\int_{\tilde\gamma} \psi\,\xi\,dS\quad\forall\xi\in V_\partial^{\rm in}\,.$$

The choice of $\pi^{\rm ex}$ and $\pi^{\rm in}$ as L^2-orthogonal projections guarantees stability in the H^s-norm, $0\le s\le 1$ and the mortar coupling term in (13) *will be*

$$b((\psi_{\rm ex},\psi_{\rm in}),(\nu,\mu))=\int_\gamma(\psi_{\rm ex}-\psi_{\rm in})\,\nu\,dS+\int_{\tilde\gamma}(\psi_{\rm in}-\psi_{\rm ex})\,\omega\,dS\quad\forall(\nu,\omega)\in V_\partial^{\rm ex}\times V_\partial^{\rm in}\,.$$

Unfortunately, in practical implementations, this choice leads to undesired difficulties due to integration of products of finite element functions defined on two different meshes. This approach would require to find intersections of edges of one mesh with the elements of the other mesh. Our choice of projection requires only to find the element of the first mesh in which a node of the second mesh is located. We do believe that the choice of projection is not very critical in this case. However, changing the projection via nodal interpolation with projection via L^2-orthogonal projection is under investigation.

4.4 Newton's method for (13)

Note that $\mathsf{a}^{\rm ex}(\cdot,\cdot)$ (resp. $\mathsf{a}^{\rm in}(\cdot,\cdot)$) in (13) is linear in the second argument but not in the first, due to the non-linear dependence of the physical coefficient μ (resp. of $\mathsf{J}_{\rm p}$) on the solution ψ. Hence, we will use Newton-type methods to find solutions of the discrete problem associated with (13). This amounts to iterate the following update rule for $(\psi_{\rm ex}^{k+1},\psi_{\rm in}^{k+1})$ and $(\lambda_{\rm ex}^{k+1},\lambda_{\rm in}^{k+1})$:

$$\begin{aligned}
d_{\psi_{\rm ex}}\mathsf{a}^{\rm ex}(\psi_{\rm ex}^k,v)(\psi_{\rm ex}^{k+1}-\psi_{\rm ex}^k)\;&+d_{\psi_{\rm in}}\mathsf{a}^{\rm in}(\psi_{\rm in}^k,w)(\psi_{\rm in}^{k+1}-\psi_{\rm in}^k)+\\
\mathsf{b}((v,w),(\lambda_{\rm ex}^{k+1},\lambda_{\rm in}^{k+1}))&=\ell(\vec I,v)-\mathsf{a}^{\rm m}((\psi_{\rm ex}^k,\psi_{\rm in}^k),(v,w))\quad\forall(v,w)\in V^{\rm ex}\times V^{\rm in},\\
\mathsf{b}((\psi_{\rm ex}^{k+1},\psi_{\rm in}^{k+1}),(\nu,\omega))&=0,\qquad\qquad\forall(\nu,\omega)\in V_\partial^{\rm ex}\times V_\partial^{\rm in}\,,
\end{aligned}$$

For the non-linear mapping $\mathsf{a}^{\rm ex}(\cdot,\cdot)$, taking into account (3), we have

$$\begin{aligned}
d_\psi\mathsf{a}^{\rm ex}(\psi,\xi)(\widetilde\psi)=&\mathsf{c}(\widetilde\psi,\xi)+\int_{\Omega^{\rm ex}}\frac{1}{\mu(\psi)r}\nabla\widetilde\psi\cdot\nabla\xi\,drdz\\
&-2\int_{\Omega_{\rm Fe}}\frac{\mu'_{\rm Fe}(|\nabla\psi|^2r^{-2})}{\mu^2_{\rm Fe}(|\nabla\psi|^2r^{-2})r^3}\nabla\widetilde\psi\cdot\nabla\psi\,\nabla\psi\cdot\nabla\xi\,drdz.
\end{aligned}$$

and for the non-linear mapping $\mathsf{a}^{\rm in}(\cdot,\cdot)$, we have

$$d_\psi\mathsf{a}^{\rm in}(\psi,\xi)(\widetilde\psi)=\int_{\Omega^{\rm L}}\frac{1}{\mu_0 r}\nabla\widetilde\psi\cdot\nabla\xi\,drdz+\mathsf{J}'_{\rm p}(\psi;\xi,\widetilde\psi)\,,\tag{15}$$

where $\mathsf{J}'_{\mathrm{p}}(\psi;\xi,\widetilde{\psi})$ is the approximation of the derivative

$$\begin{aligned} d_\psi \mathsf{J}_{\mathrm{p}}(\psi,\xi)(\widetilde{\psi}) = \int_{\Omega_{\mathrm{p}}(\psi)} \left(r S'_{p'}(\psi_{\mathrm{N}}(\psi)) + \frac{1}{\mu_0 r} S'_{ff'}(\psi_{\mathrm{N}}(\psi)) \right) d_\psi \psi_{\mathrm{N}}(\psi)(\widetilde{\psi})\, \xi \, dr dz, \\ - \int_{\partial\Omega_{\mathrm{p}}(\psi)} \left(r S_{p'}(1) + \frac{1}{\mu_0 r} S_{ff'}(1) \right) |\nabla\psi|^{-1} (\widetilde{\psi} - \widetilde{\psi}(r_{\mathrm{bd}}(\psi), z_{\mathrm{bd}}(\psi)))\xi \, d\Gamma \end{aligned} \tag{16}$$

given in [7, Lemma I.4], where

$$(d_\psi \psi_{\mathrm{N}}(\psi)(\widetilde{\psi}))(r,z) = \frac{\widetilde{\psi}(r,z) - \psi_{\mathrm{N}}(\psi)\widetilde{\psi}(r_{\mathrm{bd}}(\psi), z_{\mathrm{bd}}(\psi)) - (1-\psi_{\mathrm{N}}(\psi))\widetilde{\psi}(r_{\mathrm{ax}}(\psi), z_{\mathrm{ax}}(\psi))}{\psi_{\mathrm{bd}}(\psi) - \psi_{\mathrm{ax}}(\psi)} .$$

The derivation involves shape calculus [38, 16] and the non-trival derivatives:

$$d_\psi \psi_{\mathrm{ax}}(\psi)(\widetilde{\psi}) = \widetilde{\psi}(r_{\mathrm{ax}}(\psi), z_{\mathrm{ax}}(\psi)) \text{ and } d_\psi \psi_{\mathrm{bd}}(\psi)(\widetilde{\psi}) = \widetilde{\psi}(r_{\mathrm{bd}}(\psi), z_{\mathrm{bd}}(\psi)) .$$

There are two different approaches to introduce approximations $\mathsf{J}'_{\mathrm{p}}(\psi;\xi,\widetilde{\psi})$ of the derivative of the non-linear mapping $\mathsf{J}_{\mathrm{p}}(\psi,\xi)(\widetilde{\psi})$. The first replaces in the analytic expression (16) of the derivative the integration with standard quadrature rules. The second introduces numerical quadrature to approximate the integrals in the analytical expression (9) of the non-linear mapping and uses the analytical derivative of this approximation. While in many cases, including the derivatives of $\mathsf{a}^{\mathrm{ex}}(\psi,\xi)$, the two approaches yield the same approximation, this is not the case for $\mathsf{J}_{\mathrm{p}}(\psi,\xi)$ and we refer to [28, Section 3] for a detailed discussion on this topic. As one generally establishes convergence of numerical solutions of a discretization of a non-linear problem towards the exact solution, it is more natural to follow the second approach and to calculate analytically derivatives of discretized non-linear mappings.

We use Gauss-Legendre quadrature of order 5 for integrals on rectangles. Moreover, in the approximation of

$$\mathsf{J}_{\mathrm{p}}(\psi,\xi) = \int_{\Omega_{\mathrm{p}}(\psi)} \left(r S_{p'}(\psi_{\mathrm{N}}) + \frac{1}{\mu_0 r} S_{ff'}(\psi_{\mathrm{N}}) \right) \xi \, dr dz$$

we do not compute exactly the intersection $K \cap \Omega_{\mathrm{p}}(\psi)$ of an element K with the plasma domain $\Omega_{\mathrm{p}}(\psi)$, but extend $S_{p'}(\psi_{\mathrm{N}})$ and $S_{ff'}(\psi_{\mathrm{N}})$ by zero when $\psi_{\mathrm{N}} > 1$. Assuming that $S_{p'}(\cdot)$ and $S_{ff'}(\cdot)$ are smooth mappings from $\mathbb{R}_+$ to $\mathbb{R}_+$ we can use indeed standard quadrature rules on the rectangular elements K.

Let us underline that the second term on the righthand side of (16) vanishes whenever $j_{\mathrm{p}}(\cdot,1) = 0$. Moreover, the second and third term of $d_\psi \psi_{\mathrm{ax}}(\psi)(\widetilde{\psi})$ make $d_\psi \mathsf{J}_{\mathrm{p}}(\psi,\xi)(\widetilde{\psi})$ non-local in the sense that it does not vanish for ξ and $\widetilde{\psi}$ with disjoint supports, whenever $(r_{\mathrm{ax}}(\psi), z_{\mathrm{ax}}(\psi))$ or $(r_{\mathrm{bd}}(\psi), z_{\mathrm{bd}}(\psi))$, respectively, is in the support of $\widetilde{\psi}$.

The computation of $(r_{\mathrm{ax}}(\psi^{\mathrm{in}}), z_{\mathrm{ax}}(\psi^{\mathrm{in}}))$ and $(r_{\mathrm{bd}}(\psi^{\mathrm{in}}), z_{\mathrm{bd}}(\psi^{\mathrm{in}}))$ for a piecwise bicubic polynomial $\psi^{\mathrm{in}} \in V^{\mathrm{in}}$ is much more evolved than in the case of linear Lagrangian elements. Indeed, with piecewise linear Lagrangian elements, the critical points are located at nodes of the mesh, whereas with high-order finite elements, they occupy a position that does not coincide necessarily with a node but can be at the interior of an element. For the determination of $(r_{\mathrm{ax}}(\psi^{\mathrm{in}}), z_{\mathrm{ax}}(\psi^{\mathrm{in}}))$ we look first for the maximum of ψ^{in} at a finite number of evenly distributed points. Such an initial guess is then refined by looking for a critical point in the neighborhood which can be accomplished with standard algorithms for constrained optimization problems, where the objective is the minimization of $|\nabla\psi^{\mathrm{in}}|^2/2$. For the determination of saddle points of $\psi^{\mathrm{in}} \in V^{\mathrm{in}}$ we

interpolate ψ^{in} first onto the lower dimensional bilinear finite element space and compute the saddle points for this representation. Then we refine the location by solving again a constrained minimization problem.

4.5 Algebraic Newton iterations

By the definition of V^{ex} and V^{in} there are finite element space $V_\circ^{\text{ex}}$ and $V_\circ^{\text{in}}$ such that

$$V^{\text{ex}} = V_\circ^{\text{ex}} \oplus \mathcal{E} V_\partial^{\text{ex}} \quad \text{and} \quad V^{\text{in}} = V_\circ^{\text{in}} \oplus \mathcal{E} V_\partial^{\text{in}},$$

where $\mathcal{E}$ denotes the trivial extension operators. The elements of $V_\circ^{\text{ex}}$ and $V_\circ^{\text{in}}$ have vanishing Dirichlet trace on γ and $\tilde{\gamma}$, respectively. Then if $\mathbf{u}^{\text{ex}}$ and $\mathbf{u}^{\text{in}}$ represent the vector of degrees of freedom of $\psi^{\text{ex}} \in V^{\text{ex}}$ and $\psi^{\text{in}} \in V^{\text{in}}$ we have the decomposition $\mathbf{u}^{\text{ex}} = (\mathbf{u}_\circ^{\text{ex}}, \mathbf{u}_\partial^{\text{ex}})$ and $\mathbf{u}^{\text{in}} = (\mathbf{u}_\circ^{\text{in}}, \mathbf{u}_\partial^{\text{in}})$, where $\mathbf{u}_\circ^{\text{ex}}$ ($\mathbf{u}_\circ^{\text{in}}$) and $\mathbf{u}_\partial^{\text{ex}}$ ($\mathbf{u}_\partial^{\text{in}}$) are the degrees of freedom in $V_\circ^{\text{ex}}$ ($V_\circ^{\text{in}}$) and V_∂^{ex} (V_∂^{in}).

The matrix form of conditions (11) and (12) thus read, respectively:

$$\mathbf{u}_\partial^{\text{in}} = \mathbf{P}_{\partial,\circ}^{\text{in}} \mathbf{u}_\circ^{\text{ex}} + \mathbf{P}_{\partial,\partial}^{\text{in}} \mathbf{u}_\partial^{\text{ex}}, \qquad \mathbf{u}_\partial^{\text{ex}} = \mathbf{P}_{\partial,\circ}^{\text{ex}} \mathbf{u}_\circ^{\text{in}} + \mathbf{P}_{\partial,\partial}^{\text{ex}} \mathbf{u}_\partial^{\text{in}} \tag{17}$$

and the weak formulation (13) is the following non-linear algebraic system:

$$\begin{aligned}
\mathbf{A}_\circ^{\text{ex}}(\mathbf{u}_\circ^{\text{ex}}, \mathbf{u}_\partial^{\text{ex}}) - \left(\mathbf{P}_{\partial,\circ}^{\text{in}}\right)^T \boldsymbol{\lambda}_\partial^{\text{in}} &= \mathbf{F}_\circ^{\text{ex}} \\
\mathbf{A}_\partial^{\text{ex}}(\mathbf{u}_\circ^{\text{ex}}, \mathbf{u}_\partial^{\text{ex}}) + \boldsymbol{\lambda}_\partial^{\text{ex}} - \left(\mathbf{P}_{\partial,\partial}^{\text{in}}\right)^T \boldsymbol{\lambda}_\partial^{\text{in}} &= \mathbf{F}_\partial^{\text{ex}} \\
\mathbf{A}_\circ^{\text{in}}(\mathbf{u}_\circ^{\text{in}}, \mathbf{u}_\partial^{\text{in}}) - \left(\mathbf{P}_{\partial,\circ}^{\text{ex}}\right)^T \boldsymbol{\lambda}_\partial^{\text{ex}} &= \mathbf{0} \\
\mathbf{A}_\partial^{\text{in}}(\mathbf{u}_\circ^{\text{in}}, \mathbf{u}_\partial^{\text{in}}) + \boldsymbol{\lambda}_\partial^{\text{in}} - \left(\mathbf{P}_{\partial,\partial}^{\text{ex}}\right)^T \boldsymbol{\lambda}_\partial^{\text{ex}} &= \mathbf{0} \\
\mathbf{u}_\partial^{\text{ex}} - \mathbf{P}_{\partial,\circ}^{\text{ex}} \mathbf{u}_\circ^{\text{in}} - \mathbf{P}_{\partial,\partial}^{\text{ex}} \mathbf{u}_\partial^{\text{in}} &= \mathbf{0} \\
\mathbf{u}_\partial^{\text{in}} - \mathbf{P}_{\partial,\circ}^{\text{in}} \mathbf{u}_\circ^{\text{ex}} - \mathbf{P}_{\partial,\partial}^{\text{in}} \mathbf{u}_\partial^{\text{ex}} &= \mathbf{0}
\end{aligned} \tag{18}$$

where $\mathbf{A}_\circ^{\text{ex}}(\mathbf{u}_\circ^{\text{ex}}, \mathbf{u}_\partial^{\text{ex}})$ and $\mathbf{A}_\partial^{\text{ex}}(\mathbf{u}_\circ^{\text{ex}}, \mathbf{u}_\partial^{\text{ex}})$ is the discretization of the non-linear mapping $\mathsf{a}^{\text{ex}}(\cdot,\cdot)$ and $\mathbf{A}_\circ^{\text{in}}(\mathbf{u}_\circ^{\text{in}}, \mathbf{u}_\partial^{\text{in}})$ and $\mathbf{A}_\partial^{\text{in}}(\mathbf{u}_\circ^{\text{in}}, \mathbf{u}_\partial^{\text{in}})$ is the discretization of the non-linear mapping $\mathsf{a}^{\text{in}}(\cdot,\cdot)$.

Newton's method is used to solve iteratively the non-linear algebraic system (18). In each iteration we solve a linear system of the following form:

$$\begin{pmatrix}
\mathbf{A}_{\circ,\circ}^{\text{ex}} & \mathbf{A}_{\circ,\partial}^{\text{ex}} & 0 & 0 & 0 & -\mathbf{P}_{\partial,\circ}^{\text{in}^T} \\
\mathbf{A}_{\partial,\circ}^{\text{ex}} & \mathbf{A}_{\partial,\partial}^{\text{ex}} & 0 & 0 & \mathbf{I}_{\partial,\partial}^{\text{ex}} & -\mathbf{P}_{\partial,\partial}^{\text{in}^T} \\
0 & 0 & \mathbf{A}_{\circ,\circ}^{\text{in}} & \mathbf{A}_{\circ,\partial}^{\text{in}} & -\mathbf{P}_{\circ,\partial}^{\text{ex}^T} & 0 \\
0 & 0 & \mathbf{A}_{\partial,\circ}^{\text{in}} & \mathbf{A}_{\partial,\partial}^{\text{in}} & -\mathbf{P}_{\partial,\partial}^{\text{ex}^T} & \mathbf{I}_{\partial,\partial}^{\text{in}} \\
0 & \mathbf{I}_{\partial,\partial}^{\text{ex}} & -\mathbf{P}_{\partial,\circ}^{\text{ex}} & -\mathbf{P}_{\partial,\partial}^{\text{ex}} & 0 & 0 \\
-\mathbf{P}_{\partial,\circ}^{\text{in}} & -\mathbf{P}_{\partial,\partial}^{\text{in}} & 0 & \mathbf{I}_{\partial,\partial}^{\text{in}} & 0 & 0
\end{pmatrix}
\begin{pmatrix}
\Delta\mathbf{u}_\circ^{\text{ex}} \\ \Delta\mathbf{u}_\partial^{\text{ex}} \\ \Delta\mathbf{u}_\circ^{\text{in}} \\ \Delta\mathbf{u}_\partial^{\text{in}} \\ \boldsymbol{\lambda}_\partial^{\text{ex}} \\ \boldsymbol{\lambda}_\partial^{\text{in}}
\end{pmatrix} =
\begin{pmatrix}
\mathbf{F}_\circ^{\text{ex}} - \mathbf{A}_\circ^{\text{ex}}(\mathbf{u}_\circ^{\text{ex}}, \mathbf{u}_\partial^{\text{ex}}) \\
\mathbf{F}_\partial^{\text{ex}} - \mathbf{A}_\partial^{\text{ex}}(\mathbf{u}_\circ^{\text{ex}}, \mathbf{u}_\partial^{\text{ex}}) \\
-\mathbf{A}_\circ^{\text{in}}(\mathbf{u}_\circ^{\text{in}}, \mathbf{u}_\partial^{\text{in}}) \\
-\mathbf{A}_\partial^{\text{in}}(\mathbf{u}_\circ^{\text{in}}, \mathbf{u}_\partial^{\text{in}}) \\
\mathbf{P}_{\partial,\circ}^{\text{ex}} \mathbf{u}_\circ^{\text{in}} + \mathbf{P}_{\partial,\partial}^{\text{ex}} \mathbf{u}_\partial^{\text{in}} - \mathbf{u}_\partial^{\text{ex}} \\
\mathbf{P}_{\partial,\circ}^{\text{in}} \mathbf{u}_\circ^{\text{ex}} + \mathbf{P}_{\partial,\partial}^{\text{in}} \mathbf{u}_\partial^{\text{ex}} - \mathbf{u}_\partial^{\text{in}}
\end{pmatrix}. \tag{19}$$

The different blocks $\mathbf{A}_{\circ,\circ}^{\text{ex}}$, $\mathbf{A}_{\circ,\partial}^{\text{ex}}$, $\mathbf{A}_{\partial,\circ}^{\text{ex}}$, $\mathbf{A}_{\partial,\partial}^{\text{ex}}$ (resp. $\mathbf{A}_{\circ,\circ}^{\text{in}}$, $\mathbf{A}_{\circ,\partial}^{\text{in}}$, $\mathbf{A}_{\partial,\circ}^{\text{in}}$, $\mathbf{A}_{\partial,\partial}^{\text{in}}$) correspond to the derivatives of the discretized non-linear mappings $\mathsf{a}^{\text{ex}}(\cdot,\cdot)$ (resp. $\mathsf{a}^{\text{in}}(\cdot,\cdot)$) that we introduced in (14).

5 Numerical results

In this section we present some numerical results that highlight the features of the proposed method. We start with examples that show qualitatively the feasibility of the overlapping mortar

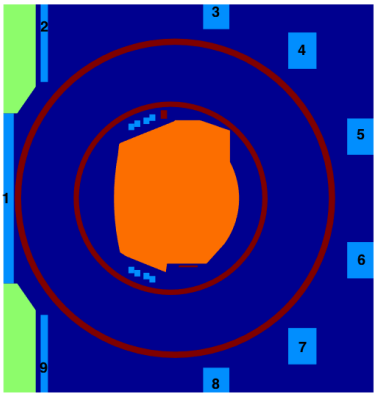

id	current	id	current
1	0	10	54000
2	0	11	54000
3	0	12	54000
4	28800	13	66000
5	−239040	14	66000
6	−239040	15	66000
7	−288000	16	66000
8	0		
9	0		

Figure 2: The values of the current (in At) for then numerical tests with the WEST tokamak. The small coils close to the vacuum chamber are numbered 10 to 16 going from left to right and top to bottom.

method. Next we study numerically the dependence of the location of critical points, such as saddle points and maximas, on the values of the currents in the poloidal field coils. This is a very important application for scenario design in tokamaks. We finish this section by presenting results for the so called geometric coefficients, certain level line integrals, which are important for the simulations of transient plasmas in tokamaks.

All subsequent examples are based on the WEST tokamak (see Figure **??** for a sketch of the different subdomains Ω_{L}, Ω_{c_i} and Ω_{Fe}). The imposed currents and the numbering of the coils can be inferred from Figure 2. For parameters in the current profile (7) we chose $\alpha = 0.9$, $\beta = 1.5$, $\gamma = 0.9$, $\lambda = 1806600$ and $R_0 = 2.4$.

5.1 Feasibility

We refer to [13, Section 5] for convergence studies on a linear problem using a similar MEM. A crucial difficulty in the here considered free-boundary equilibrium problems is a good initial guess of the plasma domain $\Omega_{\mathrm{p}}(\psi)$ for some given set of currents in the poloidal field coils. It is common to find such initial guesses by trial and error. More sophisticated approaches are based on the formulation of inverse problems or optimal control problems, where a desired shape and position of the plasma domain is the objective and the precise values of the currents is unknown [7, 28]. In the present case we do not want to focus on this technical issue, but assume we have a good initial guess for the poloidal flux ψ, e.g. from a non-mortar formulation of the free boundary equilibrium problem that is based on linear Lagrangian finite elements (which we refer to as P1 ref. in the following). In Figure (3) we show the contour plots of the solution of the mortar method (13) for an increasing number of elements of the interior rectangular mesh τ^{in}. Not very surprisingly the solutions do not differ much and are close to the reference one without MEM. The visualization in Figure 4 emphasizes this observation in focusing on the plasma boundary and the data in Table 1 give more quantitative evidence. We need less than 10 Newton iterations to reduce the relative residuum of the non-linear discrete system to values below 10^{-12}.

As we couple linear Lagrangian finite elements with Bogner-Fox-Schmit (BFS) elements, we can not expect that the solution by the MEM is significantly more accurate than the solution without MEM which relies on linear Lagrangian finite elements everywhere. It is merely the higher order regularity of the numerical solution in the vicinity of the plasma domain that

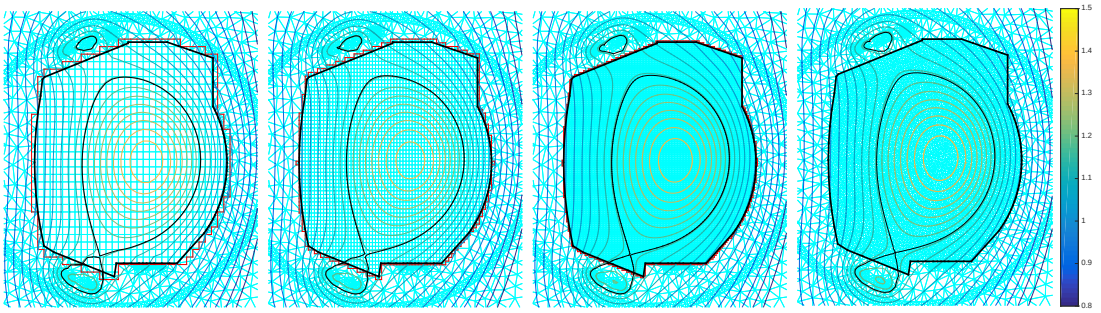

Figure 3: Contour plots of the solution by the MEM (13) and Bogner-Fox-Schmit elements (BFS) for an increasing number of elements in the interior rectangular mesh τ^{in} (1st, 2nd and 3rd from the left) and a reference solution without MEM but with linear Lagrangian finite elements.

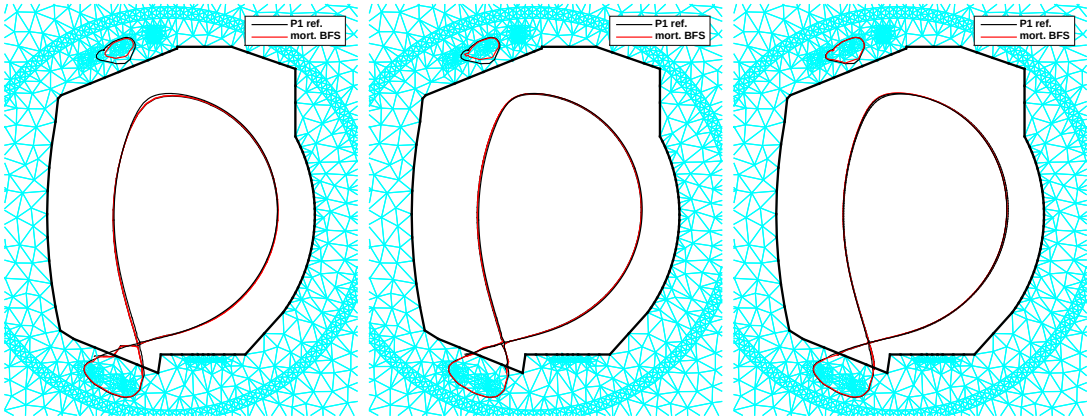

Figure 4: The ψ_{bd}-level lines of the solution by the MEM (13) for an increasing number of elements in the interior rectangular mesh τ^{in} (1st, 2nd and 3rd from the left) in comparison with ψ_{bd}-level lines for the reference solution.

renders the proposed approach so useful for practical applications as we show in the following example.

5.2 Movement of $(r_{\text{ax}}, z_{\text{ax}})$ and $(r_{\text{bd}}, z_{\text{bd}})$

In this example we are running a sequence of 30 simulations where all currents except one, namely the current in coil 4, are set to the values in the table of Figure 2. The current in coil 4 goes through uniform steps from $I_4 = 28800\,\text{At}$ to $I_4 = 104965\,\text{At}$. This test case mimics the evolution of a plasma induced by the variation of currents in time. In the conforming case with linear Lagrangian elements the magnetic axis $(r_{\text{ax}}, z_{\text{ax}})$ and the plasma boundary defining point $(r_{\text{bd}}, z_{\text{bd}})$ undergo a discontinuous evolution as their location is inherently restricted to vertices of the mesh. With the MEM we are able to introduce finite element functions in Ω^{in} that are not only continuous but have also continuous derivatives, hence the location of critical points is no more restricted to a finite number of points. This reasoning agrees perfectly with the observations. In Figure 5 we see that the evolution of the perturbations $(\Delta r_{\text{ax}}, \Delta z_{\text{ax}})$ and $(\Delta r_{\text{bd}}, \Delta z_{\text{bd}})$ of magnetic axis and boundary defining point evolve smoothly with the current

	$r_{\mathrm{ax}}(m)$	$z_{\mathrm{ax}}(m)$	$\psi_{\mathrm{ax}}(Wb)$	$r_{\mathrm{bd}}(m)$	$z_{\mathrm{bd}}(m)$	$\psi_{\mathrm{bd}}(Wb)$
1	2.5843	0.0073	1.3949	2.2646	−0.6197	1.1614
2	2.5799	0.0160	1.3890	2.2726	−0.6174	1.1582
3	2.5842	0.0163	1.3959	2.2794	−0.6158	1.1641
P1 ref.	2.5879	0.0026	1.3968	2.2795	−0.6125	1.1652

Table 1: Location of the magnetic axis and the plasma boundary defining point with the MEM for three different choices of the mesh τ^{in} (see Figure 3) and the corresponding values for the solution without the MEM at the bottom line.

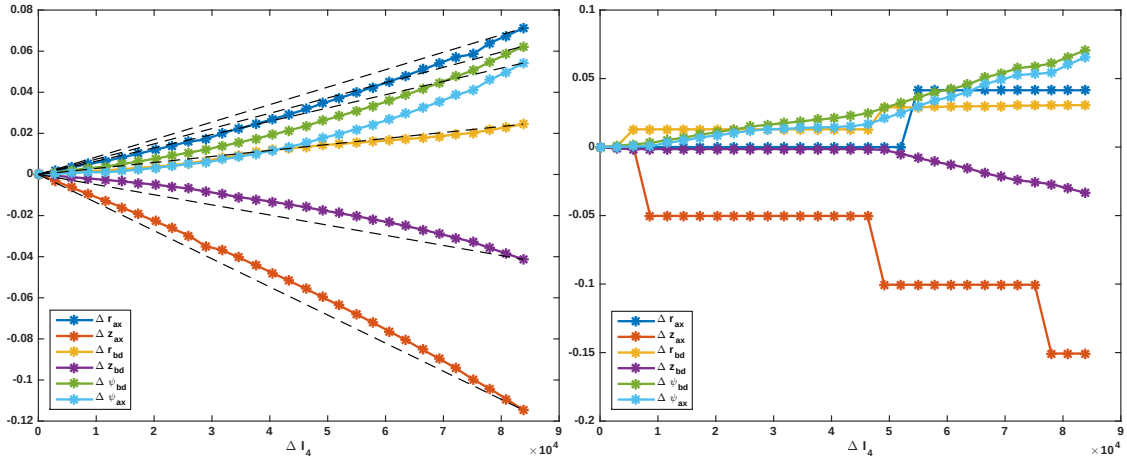

Figure 5: Evolution of the perturbations $(\Delta r_{\mathrm{ax}}, \Delta z_{\mathrm{ax}})$ and $(\Delta r_{\mathrm{bd}}, \Delta z_{\mathrm{bd}})$ of the magnetic axis and the boundary defining point w.r.t. the current perturbation ΔI_4: the MEM (13) with the Bogner-Fox-Schmit element (left) and the MEM with bilinear finite elements instead of the Bogner-Fox-Schmit elements (right).

perturbation. To highlight the influence of the continuous derivatives we compare the results with a mortar methods that uses bilinear finite elements (Q1) instead of the bicubic Bogner-Fox-Schmit elements. Maxima and mimima of bilinear finite element functions are again necessarily on vertices of the mesh, while saddle points can lie either on vertices or inside an element (see Figure 5 right). We would like to stress that the evolution of the perturbations $\Delta\psi_{\mathrm{ax}}$ and $\Delta\psi_{\mathrm{bd}}$ of the values of ψ at the magnetic axis and the boundary defining point is smooth in both cases. The discontinuous behavior of the location of critical points is not inherited to the values of ψ_h at its critical points.

The visualization in Figure 6 stresses the undesired behavior that appears due to non-continuous gradients and shows how this defect can be cured by using the Bogner-Fox-Schmit finite element.

5.3 Geometric Coefficients

A very important output of equilibrium calculations are the so called geometric coefficients. The Grad/Hogan approach [23] to the simulation of evolution of plasma in a tokamak on very long timescales, asserts that the fluid model quantities such as densities or temperatures are constant on the level lines of the poloidal flux. Hence, transforming the corresponding conservation laws

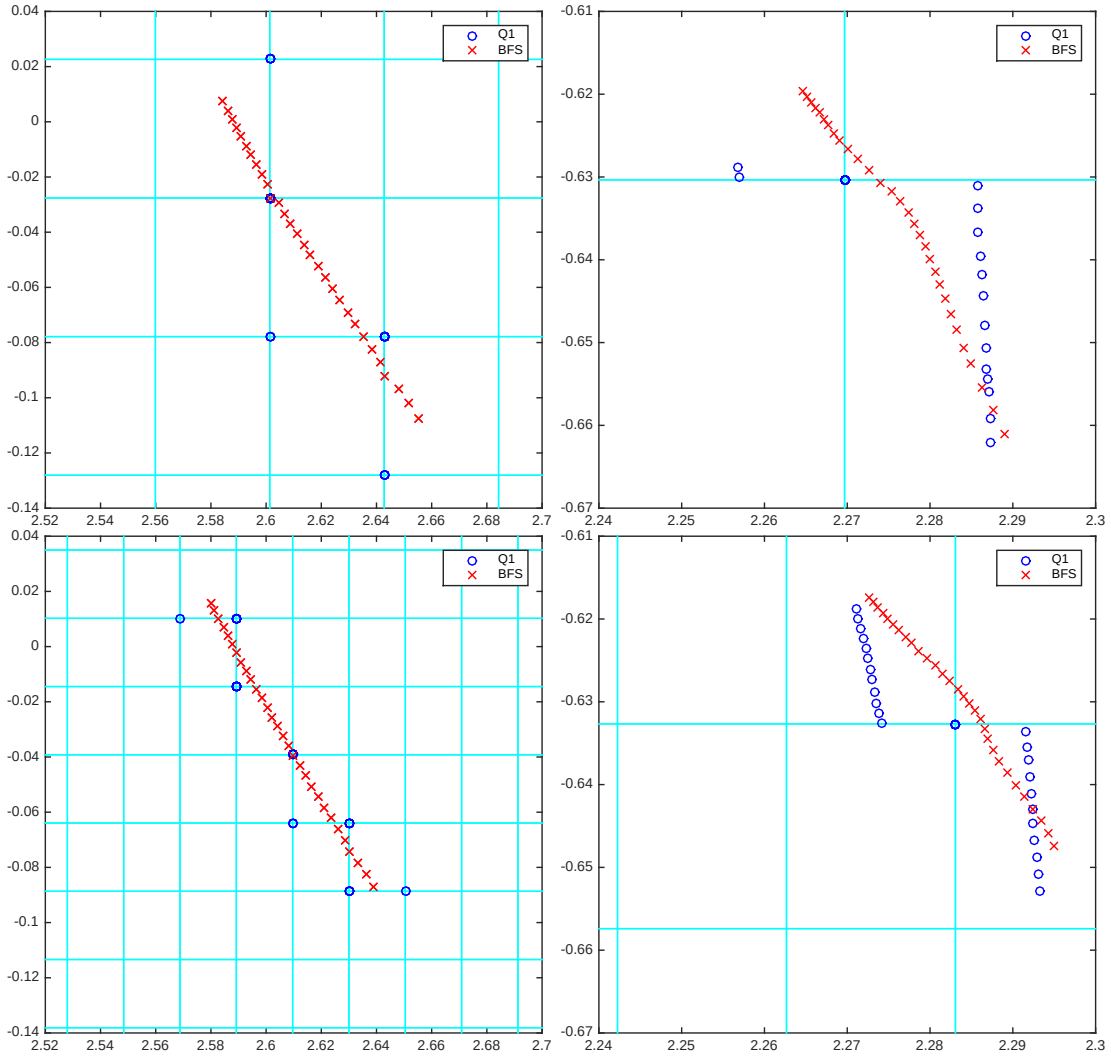

Figure 6: Locations of $(r_{\mathrm{ax}}, z_{\mathrm{ax}})$ (left) and $(r_{\mathrm{bd}}, z_{\mathrm{bd}})$ (right) for a variation ΔI_4 of the current in coil 4. Simulations are done on a mesh (top) and on a refinement of it (bottom). The solution with bilinear finite elements (Q1) is compared with the numerical solution using the Bogner-Fox-Schmit finite element (BFS).

into a curvilinear coordinate system with one coordinate line aligned with the level lines of the poloidal flux ψ, we end up with a system of one dimensional equations, with metric coefficients due to the non-linear coordinate transformation. As the coordiante transformation depends on ψ, also the metric coefficients depend on ψ. In the tokamak literature these coefficients are referred to as *geometric coefficients* (see [9] for a concise introduction to this topic focusing on numerical methods). The Grad/Hogan approach is implemented in many productive simulation tools [34, 15, 49, 29] that are used to study the evolution of plasma in tokamaks.

More precisely, the *geometric coefficients* are non-linear functionals of the following form

$$g_{f,\psi_{\mathrm{N}}}(y) = \int\limits_{\{(r,z)\in\Omega_{\mathrm{p}}(\psi),\, \psi_{\mathrm{N}}(r,z)=y\}} \frac{f(r,z)r}{|\nabla\psi_{\mathrm{N}}(r,z)|}ds\,. \tag{20}$$

that, for given smooth scalar functions $f : \Omega \to \mathbb{R}$, are integrals along the level line $\{(r,z) \in \Omega, \psi_{\mathrm{N}}(r,z) = y\}$. For the numerical approximation of $g_{f,\psi_{\mathrm{N}}}(y)$ we need to find the elements that intersect with the level line $\{(r,z) \in \Omega, \psi^{\mathrm{in}}_{\mathrm{N}}(r,z) = y\}$, where $\psi^{\mathrm{in}}_{\mathrm{N}}$ is the normalization based on $\psi^{\mathrm{in}} \in V^{\mathrm{in}}$, the solution of the mortar-like formulation (13). Since ψ^{in} is a piecewise bicubic, we have only an implicit representation of the level line. To exploit nevertheless the high order polynomial representation of ψ^{in} we use the Simpson quadrature rule

$$\int\limits_{\{(r,z)\in\Omega_{\mathrm{p}}(\psi),\, \psi^{\mathrm{in}}_{\mathrm{N}}(r,z)=y\}\cap K} \frac{f(r,z)r}{|\nabla\psi^{\mathrm{in}}_{\mathrm{N}}(r,z)|}ds \approx$$
$$\frac{1}{6}\left(|\dot{\mathbf{s}}(t_1)|\frac{f(r_1,z_1)r_1}{|\nabla\psi^{\mathrm{in}}_{\mathrm{N}}(r_1,z_1)|} + 4|\dot{\mathbf{s}}(t_2)|\frac{f(r_2,z_2)r_2}{|\nabla\psi^{\mathrm{in}}_{\mathrm{N}}(r_2,z_2)|} + |\dot{\mathbf{s}}(t_3)|\frac{f(r_3,z_3)r_3}{|\nabla\psi^{\mathrm{in}}_{\mathrm{N}}(r_3,z_3)|}\right)$$

with $\mathbf{s}(t_1) = \mathbf{s}(0) = (r_1, r_1)$ and $\mathbf{s}(t_3) = \mathbf{s}(1) = (r_3, r_3)$ the two intersection points of the level line with ∂K. To determine the intermediate point $\mathbf{s}(t_2) = \mathbf{s}(1/2) = (r_2, r_2)$ and the tangent vectors $\dot{\mathbf{s}}(t_i)$ we follow the procedure outlined in [17, p. 199]. The intermediate point $\mathbf{s}(t_2)$ verifies the non-linear problem

$$\psi^{\mathrm{in}}_{\mathrm{N}}(r_2,z_2) = 0\,,$$
$$(1-t_2)\begin{pmatrix} r_2-r_1 \\ z_2-z_1\end{pmatrix}\cdot\begin{pmatrix} r_3-r_1 \\ z_3-z_1\end{pmatrix} + t_2\begin{pmatrix} r_2-r_3 \\ z_2-z_3\end{pmatrix}\cdot\begin{pmatrix} r_3-r_1 \\ z_3-z_1\end{pmatrix} = 0\,,$$

and the tangent vectors $\dot{\mathbf{s}}(t_i)$ are solution of the linear systems

$$\partial_r\psi^{\mathrm{in}}_{\mathrm{N}}(r_i,z_i)\dot{\mathbf{s}}_r(t_i) + \partial_z\psi^{\mathrm{in}}_{\mathrm{N}}(r_i,z_i)\dot{\mathbf{s}}_z(t_i) = 0\,,$$
$$(1-t_i)\begin{pmatrix} \mathbf{s}_r(t_i)-r_1 \\ \mathbf{s}_z(t_i)-z_1\end{pmatrix}\cdot\begin{pmatrix} r_3-r_1 \\ z_3-z_1\end{pmatrix} + t_i\begin{pmatrix} \mathbf{s}_r(t_i)-r_3 \\ \mathbf{s}_z(t_i)-z_3\end{pmatrix}\cdot\begin{pmatrix} r_3-r_1 \\ z_3-z_1\end{pmatrix} = 0\,.$$

We are validating the computation of the geometric coefficients for the following elliptical data

$$\psi^{\mathrm{E}}(r,z) = \psi_{\mathrm{ax}} - \left(\frac{(r-r_{\mathrm{ax}})^2}{a^2} + \frac{(z-z_{\mathrm{ax}})^2}{b^2}\right), \tag{21}$$

and $\psi_{\mathrm{bd}} = 0$ with parameters $a = 1$, $b = 3$, $r_{\mathrm{ax}} = 2$, $z_{\mathrm{ax}} = 0$ and $\psi_{\mathrm{ax}} = 2$. We project this data into the Bogner-Fox-Schmit finite element space for a domain $[0.1, 4] \times [-4.5, 4.5]$, then we compare the numerical values obtained for the geometric coefficients with the following analytical

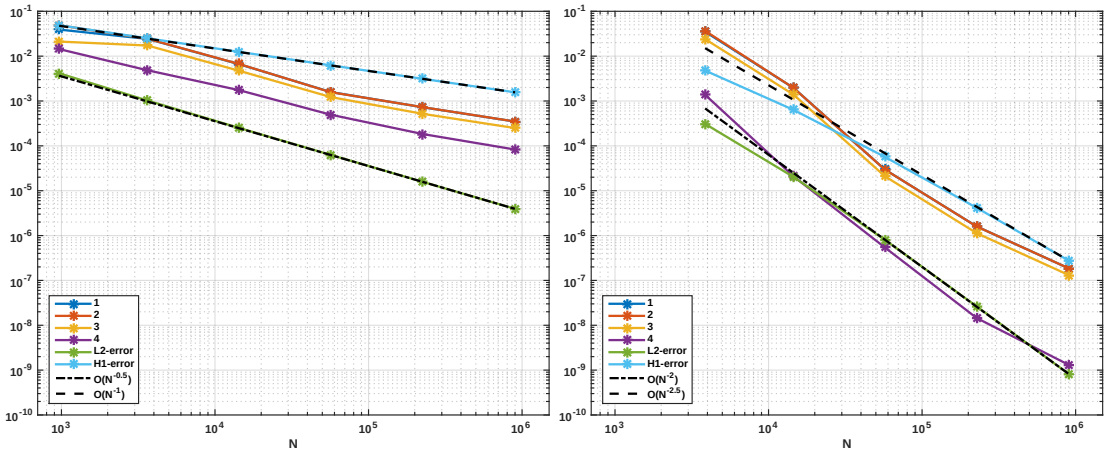

Figure 7: Convergence of the geometric coefficients for sequence of mesh refinements: bilinear finite elements (left) and Bogner-Fox-Schmit finite elements (right). The green and blue lines correspond to relative L^2_*-error and $\mathcal{H}^1$-error respectively. We monitor the maximal relative error for $g_{f,\psi_{\mathrm{E}}}(y)$ with $f = f_1 = 1/r$, $f = f_2 = 1$, $f = f_3 = 1/r^2$ and $f = f_4 = |\nabla\psi|^2/r^2$, where the maximum is taken over 40 equidistant values of y between 0 and 1. The abscissa is the number N of degrees of freedom of the finite element description of ψ,

ones:

$$
\begin{aligned}
g_{\frac{1}{r},\psi_{\mathrm{N}}^{\mathrm{E}}}(y) =& |\psi_{\mathrm{ax}}| ab\pi \,, \\
g_{1,\psi_{\mathrm{N}}^{\mathrm{E}}}(y) =& |\psi_{\mathrm{ax}}| ab\pi r_{\mathrm{ax}} \,, \\
g_{\frac{1}{r^2},\psi_{\mathrm{N}}^{\mathrm{E}}}(y) =& \frac{|\psi_{\mathrm{ax}}| ab\pi}{\sqrt{r_{\mathrm{ax}}^2 + a^2\psi_{\mathrm{ax}} y}} \,, \\
g_{\frac{|\nabla\psi^{\mathrm{E}}|^2}{r^2},\psi_{\mathrm{N}}^{\mathrm{E}}}(y) =& 4\pi|\psi_{\mathrm{ax}}| \frac{(b^2-a^2) r_{\mathrm{ax}} (r_{\mathrm{ax}} - \sqrt{r_{\mathrm{ax}}^2 + a^2\psi_{\mathrm{ax}} y}) - a^4 \psi_{\mathrm{ax}} y}{a^3 b \sqrt{r_{\mathrm{ax}}^2 + a^2\psi_{\mathrm{ax}} y}} \,.
\end{aligned}
$$

Figure 7 shows the convergence on a sequence of mesh refinements. We are computing numerically the values of the geometric coefficients at 40 equidistant values between 0 and 1 and monitor the maximal relative error. We obtain the expected high order convergence. Not very surprisingly the rate of convergence seems to correspond to the rate of convergence of the projection error for ψ^E in the $\mathcal{H}^1$-norm. Compared to bilinear finite elements we can achieve higher accuracy with the same number of unknowns.

We conclude with a comparison of the geometric coefficients for a solution obtained by the MEM coupled either with the bilinear finite element space or with the Bogner-Fox-Schmit finite element space, on a sequence of refined meshes τ^{in} (see Figure 8).

6 Conclusions and Outlook

We have presented a novel approach to introduce higher order regular finite elements for plasma equilibrium calculations in tokamaks. Higher order regular finite element spaces can be easily defined on Cartesian meshes. The MEM on overlapping meshes combines easily the finite elements on Cartesian meshes with with finite elements on triangular meshes, that in turn allow for an accurate resolution of design details in realistic geometries. It is possible to use similar ideas

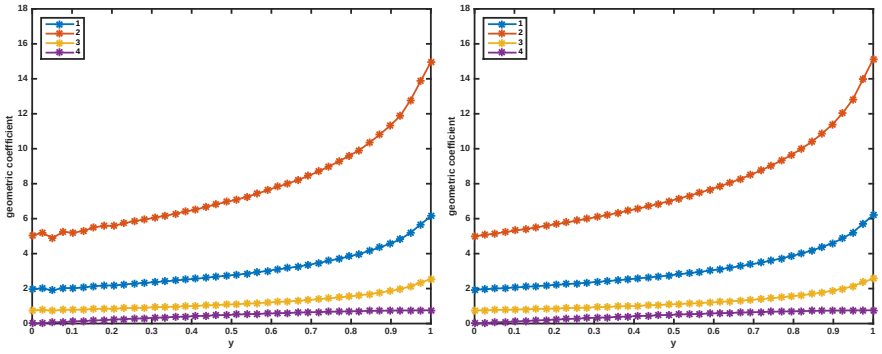

Figure 8: The geometric coefficients $g_{f,\psi^{\text{in}}}(y)$ with $f = f_1 = 1/r$, $f = f_2 = 1$, $f = f_3 = 1/r^2$ and $f = f_4 = |\nabla\psi^{\text{in}}|^2/r^2$ using the MEM (13) with either bilinear finite elements (left) or Bogner-Fox-Schmit elements (right). The small oscillations near $y = 0$ that we observe in the case of bilinear finite elements disappear when using the Bogner-Fox-Schmit elements. Clearly this comes at a prize, the larger number of unknowns, and could be also cured by using bilinear finite element on a much finer mesh.

for the coupling of more complex plasma models with eddy current modeling in coils and passive structures. Moreover, we could enforce not only continuous derivatives but also continuity for higher order derivatives, using tensor products of higher order splines to define appropriate finite element spaces in analogy to the Bogner-Fox-Schmit finite element space. Figure 9 shows a numerical result that uses a biquintic finite element space in Ω^{in} that ensures continuity of second order derivatives. Continuity of second order derivatives goes goes beyond the scope of conforming finite elements on unstructured meshes, but thanks to MEM we can provide now accurate plasma equilibrium solvers with this feature. Our main motivation for this work is more accurate computation of geometric coefficients and location of axis and boundary defining point for forthcoming simulations of the Grad/Hogan model. But there are many more applications in fusion science that can benefit from our approach. The control of the location of the plasma defining point for heat load minimization of divertor design [5, 6] or the computation of plasma equilibria with so-called snowflake configuration [43] are two of such very relevant applications.

Acknowledgments

The authors are grateful to Jacques Blum and Cedric Boulbe for stimulating discussions on plasma equilibrium problems. The second author warmly thanks the CASTOR team at INRIA Sophia-Antipolis for the delegation in 2015/2016, during which this work was completed.

References

[1] R. Albanese, J. Blum, and O. Barbieri. On the solution of the magnetic flux equation in an infinite domain. In *EPS. 8th Europhysics Conference on Computing in Plasma Physics (1986)*, pages 41–44, 1986.

[2] K. Bell. A refined triangular plate bending finite element. *International Journal for Numerical Methods in Engineering*, 1(1):101–122, 1969.

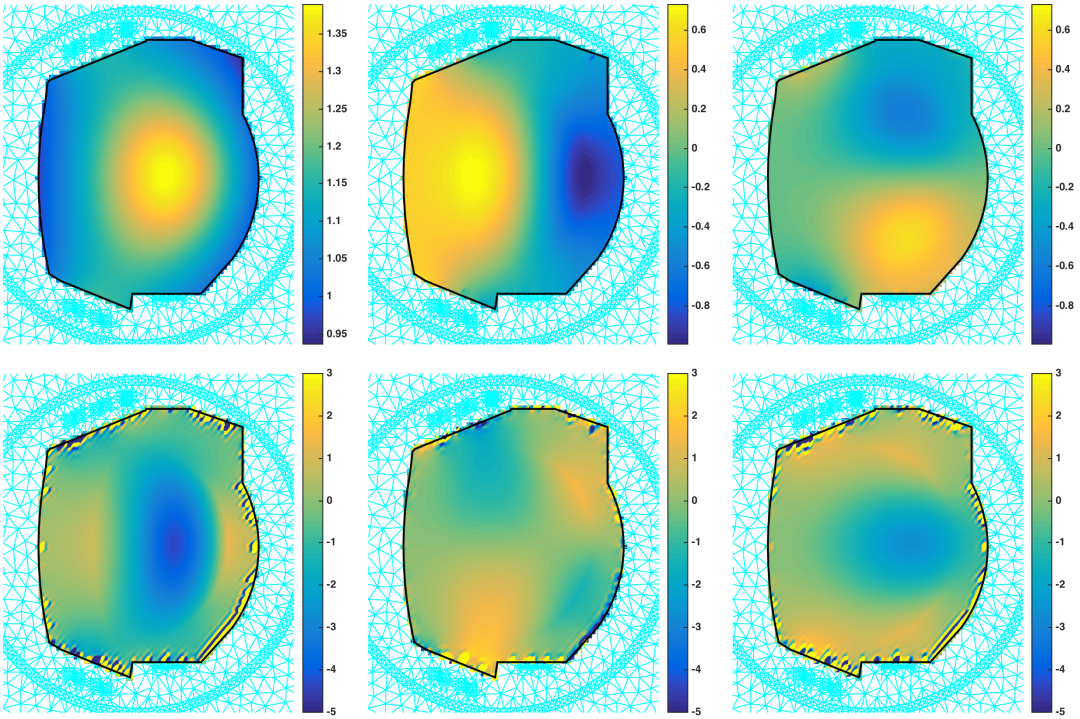

Figure 9: Numerical results with the data from Section 5 by the MEM (13) coupled with biquintic finite elements in the vacuum region instead of the bicubic Bogner-Fox-Schmit finite element. Without any post-processing, continuous second order derivatives are immediately available. The calculation is based on the second choice of the combination of meshes given in Figure 3. We show pseudo-heat plots of ψ, $\partial_r\psi$, $\partial_z\psi$, $\partial_{r,r}\psi$, $\partial_{r,z}\psi$ and $\partial_{z,z}\psi$ (from left to right, top to bottom). Sufficiently far away from the interface γ we have consistent and smooth second order information on the poloidal flux. The non-smooth artificial interface $\tilde{\gamma}$ introduces localized oscillations on the second order derivatives, only. Indeed, we are combining linear (vanishing second order derivatives) with bi-quintic (non-vanishing cubic second order derivatives) finite elements.

[3] H. Berestycki and H. Brézis. On a free boundary problem arising in plasma physics. *Nonlinear Anal.*, 4(3):415–436, 1980.

[4] C. Bernardi, Y. Maday, and A. T. Patera. A new nonconforming approach to domain decomposition: the mortar element method. In *Nonlinear partial differential equations and their applications. Collège de France Seminar, Vol. XI (Paris, 1989–1991)*, volume 299 of *Pitman Res. Notes Math. Ser.*, pages 13–51. Longman Sci. Tech., Harlow, 1994.

[5] M. Blommaert, M. Baelmans, W. Dekeyser, N.R. Gauger, and D. Reiter. A novel approach to magnetic divertor configuration design. *Journal of Nuclear Materials*, (0):–, 2014.

[6] M. Blommaert, H. Heumann, M. Baelmans, N. R. Gauger, and D. Reiter. Towards automated magnetic divertor design for optimal heat exhaust. *ESAIM: Proc.*, 53:49–63, 2016.

[7] J. Blum. *Numerical simulation and optimal control in plasma physics*. Wiley/Gauthier-Villars, 1989.

[8] J. Blum, T. Gallouet, and J. Simon. Existence and control of plasma equilibrium in a tokamak. *SIAM Journal on Mathematical Analysis*, 17(5):1158–1177, 1986.

[9] J. Blum and J. Le Foll. Plasma equilibrium evolution at the resistive diffusion timescale. *Computer Physics Reports*, 1(7-8):465–494, 1984.

[10] J. Blum, J. Le Foll, and B. Thooris. The self-consistent equilibrium and diffusion code SCED. *Computer Physics Communications*, 24:235 – 254, 1981.

[11] F. K. Bogner, R. L. Fox, and L. A. Schmit. The generation of interelement compatible stiffness and mass matrices by the use of interpolation formulas. In *Proceedings of the Conference on Matrix Methods in Structural Mechanics*, 1965.

[12] X.-C. Cai, M. Dryja, and M. Sarkis. Overlapping nonmatching grid mortar element methods for elliptic problems. *SIAM J. Numer. Anal.*, 36(2):581–606, 1999.

[13] A. Christophe, Y. Le Bihan, and F. Rapetti. A mortar element approach on overlapping non-nested grids: application to eddy current non-destructive testing. *Appl. Math. Comput.*, 267:71–82, 2015.

[14] P. G. Ciarlet. *The Finite Element Method for Elliptic Problems*. North-Holland Publishing Co., Amsterdam, 1978. Studies in Mathematics and its Applications, Vol. 4.

[15] J. A. Crotinger. Corsica; a comprehensive simulation of toroidal magnetic-fusion devices. Technical report ucrl-id-126284, Lawrence Livermore National Laboratory, 1997.

[16] M. C. Delfour and J.-P. Zolésio. *Shapes and geometries*, volume 22 of *Advances in Design and Control*. Society for Industrial and Applied Mathematics (SIAM), Philadelphia, PA, second edition, 2011.

[17] L. Demkowicz. *Computing with hp-adaptive finite elements. Vol. 1.* Chapman & Hall/CRC Applied Mathematics and Nonlinear Science Series. Chapman & Hall/CRC, Boca Raton, FL, 2007. One and two dimensional elliptic and Maxwell problems, With 1 CD-ROM (UNIX).

[18] J. P. Freidberg. *Ideal Magnetohydrodynamics*. Plenum US, 1987.

[19] G. N. Gatica and G. C. Hsiao. The uncoupling of boundary integral and finite element methods for nonlinear boundary value problems. *J. Math. Anal. Appl.*, 189(2):442–461, 1995.

[20] J. P. Goedbloed. Conformal mapping methods in two-dimensional magnetohydrodynamics. *Computer Physics Communications*, 24(3-4):311 – 321, 1981.

[21] J. P. Goedbloed, R. Keppens, and S. Poedts. *Advanced magnetohydrodynamics: with applications to laboratory and astrophysical plasmas*. Cambridge University Press, 2010.

[22] J. P. Goedbloed and S. Poedts. *Principles of magnetohydrodynamics: with applications to laboratory and astrophysical plasmas*. Cambridge university press, 2004.

[23] H. Grad and J. Hogan. Classical diffusion in a tokamak. *Phys. Rev. Lett.*, 24:1337–1340, Jun 1970.

[24] H. Grad and H. Rubin. Hydromagnetic equilibria and force-free fields. *Proceedings of the 2nd UN Conf. on the Peaceful Uses of Atomic Energy*, 31:190, 1958.

[25] V. Grandgirard. *Modélisation de l'équilibre d'un plasma de tokamak*. PhD thesis, l'Université de Franche-Comté, 1999.

[26] H. Haddar and Z. Jiang. Axisymmetric eddy current inspection of highly conducting thin layers via asymptotic models. *Inverse Problems*, 31(11):115005, 25, 2015.

[27] H. Haddar, Z. Jiang, and A. Lechleiter. Artificial boundary conditions for axisymmetric eddy current probe problems. *Computers & Mathematics with Applications*, 68(12, Part A):1844 – 1870, 2014.

[28] H. Heumann, J. Blum, C. Boulbe, B. Faugeras, G. Selig, J.-M. Ané, S. Brémond, V. Grandgirard, P. Hertout, and E. Nardon. Quasi-static free-boundary equilibrium of toroidal plasma with CEDRES++: Computational methods and applications. *Journal of Plasma Physics*, 81, 6 2015.

[29] M. Honda. Simulation technique of free-boundary equilibrium evolution in plasma ramp-up phase. *Computer Physics Communications*, 181(9):1490–1500, SEP 2010.

[30] E. C. Howell and C. R. Sovinec. Solving the Grad-Shafranov equation with spectral elements. *Computer Physics Communications*, 185(5):1415 – 1421, 2014.

[31] S. C. Jardin. A triangular finite element with first-derivative continuity applied to fusion MHD applications. *J. Comput. Phys.*, 200(1):133–152, October 2004.

[32] S. C. Jardin. *Computational methods in plasma physics*. Boca Raton, FL : CRC Press/Taylor & Francis, 2010.

[33] G. E. Karniadakis and S. J. Sherwin. *Spectral/hp element methods for computational fluid dynamics*. Numerical Mathematics and Scientific Computation. Oxford University Press, New York, second edition, 2005.

[34] R. R. Khayrutdinov and V. E. Lukash. Studies of plasma equilibrium and transport in a tokamak fusion device with the inverse-variable technique. *Journal of Computational Physics*, 109(2):193 – 201, 1993.

[35] Y. A. Kuznetsov. Overlapping domain decomposition with non-matching grids. In *Recent developments in domain decomposition methods and flow problems (Kyoto, 1996; Anacapri, 1996)*, volume 11 of *GAKUTO Internat. Ser. Math. Sci. Appl.*, pages 62–71. Gakkōtosho, Tokyo, 1998.

[36] R. Lüst and A. Schlüter. Axialsymmetrische magnetohydrodynamische Gleichgewichtskonfigurationen. *Z. Naturforsch. A*, 12:850–854, 1957.

[37] J. L. Luxon and B. B. Brown. Magnetic analysis of non-circular cross-section tokamaks. *Nuclear Fusion*, 22(6):813, 1982.

[38] F. Murat and J. Simon. Sur le contrôle par un domaine géométrique. Technical Report 76015, Laboratoire d'Analyse Numérique, Université de Paris 6, 1976.

[39] M. A. Nakamura. On an equilibrium of the plasma in a tokamak with a limiter. *Japan Journal of Industrial and Applied Mathematics*, 8(3):431–444.

[40] A. Palha, B. Koren, and F. Felici. A mimetic spectral element solver for the gradshafranov equation. *Journal of Computational Physics*, 316:63 – 93, 2016.

[41] A. Pataki, A. J. Cerfon, J. P. Freidberg, L. Greengard, and M. O'Neil. A fast, high-order solver for the grad-shafranov equation. *Journal of Computational Physics*, 243(0):28 – 45, 2013.

[42] C. Pechstein and B. Jüttler. Monotonicity-preserving interproximation of B-H-curves. *J. Comput. Appl. Math.*, 196(1):45–57, 2006.

[43] D. D. Ryutov. Geometrical properties of a snowflake divertor. *Physics of Plasmas*, 14(6), 2007.

[44] C. Schwab. *p- and hp- finite element methods : theory and applications in solid and fluid mechanics*. Oxford : Clarendon Press, 2004.

[45] V. D. Shafranov. On magnetohydrodynamical equilibrium configurations. *Soviet Journal of Experimental and Theoretical Physics*, 6:545, 1958.

[46] R. Temam. Remarks on a free boundary value problem arising in plasma physics. *Comm. Partial Differential Equations*, 2(6):563–585, 1977.

[47] J. Wesson. *Tokamaks*. The International Series of Monographs in Physics. Oxford University Press, 2004.

[48] B. I. Wohlmuth. *Discretization methods and iterative solvers based on domain decomposition*, volume 17 of *Lecture Notes in Computational Science and Engineering*. Springer-Verlag, Berlin, 2001.

[49] F. S. Zaitsev, A. G. Shishkin, D. P. Kostomarov, M. R. O'Brien, R. J. Akers, M. Gryaznevich, A.B. Trefilov, and A.S. Yelchaninov. The numerical solution of the self-consistent evolution of plasma equilibria. *Computer Physics Communications*, 157(2):107–120, FEB 15 2004.

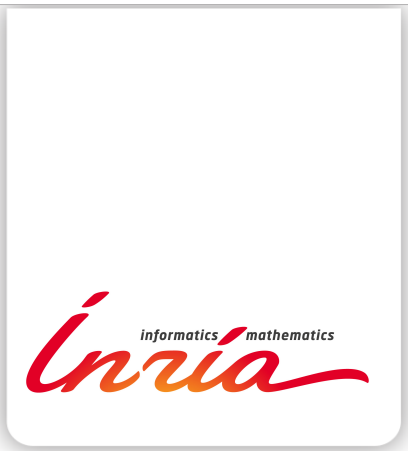

RESEARCH CENTRE
SOPHIA ANTIPOLIS – MÉDITERRANÉE

2004 route des Lucioles - BP 93
06902 Sophia Antipolis Cedex

Publisher
Inria
Domaine de Voluceau - Rocquencourt
BP 105 - 78153 Le Chesnay Cedex
inria.fr

ISSN 0249-6399